Localized and Continuous Tuning of Monolayer MoS_2 Photoluminescence Using a Single Shape-Controlled Ag Nanoantenna

Wei Gao, Yih Hong Lee, Ruibin Jiang, Jianfang Wang, Tianxi Liu, and Xing Yi Ling**

Gaining control over the nanoscale behavior of light is critical in realizing various next-generation technologies, including ultrasmall light sources,[1–3] supercomputing,[4,5] advanced optoelectronic devices,[6] and even nanoscale anticounterfeiting platforms.[7,8] Plasmonic nanomaterials are widely used in tailoring nanoscale light-matter interactions,[9–12] because they support localized surface plasmon resonances (LSPRs) which are capable of confining light into deep subwavelength volumes.[9] In addition, plasmonic nanomaterials can manipulate the light emission patterns and directions of nearby photoluminescent species.[1,13,14] Despite tremendous progress achieved in understanding the subwavelength behavior of light in this field,[15–18] it remains challenging to design a sub-micron-scale heterogeneous optical platform. On such platforms, optical signals are tightly modulated within highly confined regions, giving rise to a range of tunable optical outputs. These heterogeneous optical platforms form the basis for optical circuit components,[19] logic gates,[20] and data storage.[21]

Conversely, monolayer molybdenum disulfide (1L-MoS_2) is an emerging 2D semiconductor exhibiting photoluminescence in the visible due to its direct bandgap.[22] In contrast to other 0D and 1D emitters, the 2D nature of 1L-MoS_2 in the absence of interlayer interactions promises increased flexibility and more efficient device functionality.[23–26] 1L-MoS_2 has also been demonstrated to be an outstanding platform to investigate light-matter interactions.[27] However, 1L-MoS_2 suffers from low light absorption conferred by its sub-nm thickness, leading to photoluminescence with low quantum yields. To enhance light emission of 1L-MoS_2, various approaches, including chemical doping,[28] polymeric nanospacing,[29] defect engineering,[30] and coupling with plasmonic nanomaterials[31–33] have been employed. While these methods are relatively successful, most of them require complex fabrication steps for device integration, inadvertently introducing defects and/or modifying the intrinsic optical properties of 1L-MoS_2. In plasmonic nanomaterials coupled-1L-MoS_2 systems, plasmon-induced hot electron injection and doping have been reported to cause phase transition of 1L-MoS_2 in some cases,[34–36] with both photoluminescence quenching[37] and enhancement[31,32] observed. In addition, focus is predominantly placed on enhancing the "ensemble" optical emission of 1L-MoS_2, using lithographically fabricated Au[31] and Ag arrays,[32] close-packed Au film,[37] and Au nanoparticles.[36] To date, there is a lack of investigation exploiting the 2D nature of 1L-MoS_2 as a sub-micron-scale platform to design a heterogeneous optical platform. Furthermore, the ability of plasmonic nanomaterials to serve as highly confined nanometer-scale optical controllers in such systems has also not been fully explored.

Herein, we demonstrate the localized photoluminescence manipulation of 1L-MoS_2 using single shape-controlled plasmonic Ag nanoantenna. Our strategy focuses on using single Ag nanoantenna of various morphologies to control the extent of spectral overlap between the LSPRs of the Ag nanoantenna and the bandgap of 1L-MoS_2. This approach allows us to precisely tailor the emission response of 1L-MoS_2 by controlling the relative rates of excitation enhancement, quantum yield, and emission directionality. As such, we can continuously tune the photoluminescence of 1L-MoS_2 from an enhanced regime to a weakened state. Such weakened emission arises from both emission quenching and complex antenna effect of the Ag nanoantenna. We then realize a heterogeneous optical platform by combining various Ag nanoantennas to achieve a range of photoluminescence output signals on the same 1L-MoS_2 in highly confined nanoscale dimensions. In addition to the use of direct bandgap 1L-MoS_2, we also highlight that photoluminescence enhancement can be achieved on few-layer MoS_2 with indirect bandgaps in our system.

We first mechanically exfoliate bulk MoS_2 into few and monolayers to study the thickness-dependent evolution of its intrinsic optical properties. Optical microscopy and atomic force microscopy (AFM) are used to identify the ultrathin MoS_2 layers, as well as confirm the layer number from monolayer (1L) to quadrilayer (4L) (**Figure 1**A and Figure S1A,B, Supporting Information). These MoS_2 layers exhibit thickness-dependent

W. Gao, Dr. Y. H. Lee, Prof. X. Y. Ling
Division of Chemistry and Biological Chemistry
School of Physical and Mathematical Sciences
Nanyang Technological University
Singapore 637371
E-mail: xyling@ntu.edu.sg
W. Gao, Prof. T. Liu
State Key Laboratory of Molecular Engineering of Polymers
Department of Macromolecular Science
Fudan University
Shanghai 200433, P. R. China
E-mail: txliu@fudan.edu.cn
Prof. R. B. Jiang, Prof. J. F. Wang
Department of Physics
The Chinese University of Hong Kong
Shatin, Hong Kong SAR, China
Prof. R. B. Jiang
School of Materials Science and Engineering
Shaanxi Normal University
Xi'an 710119, P. R. China

DOI: 10.1002/adma.201503905

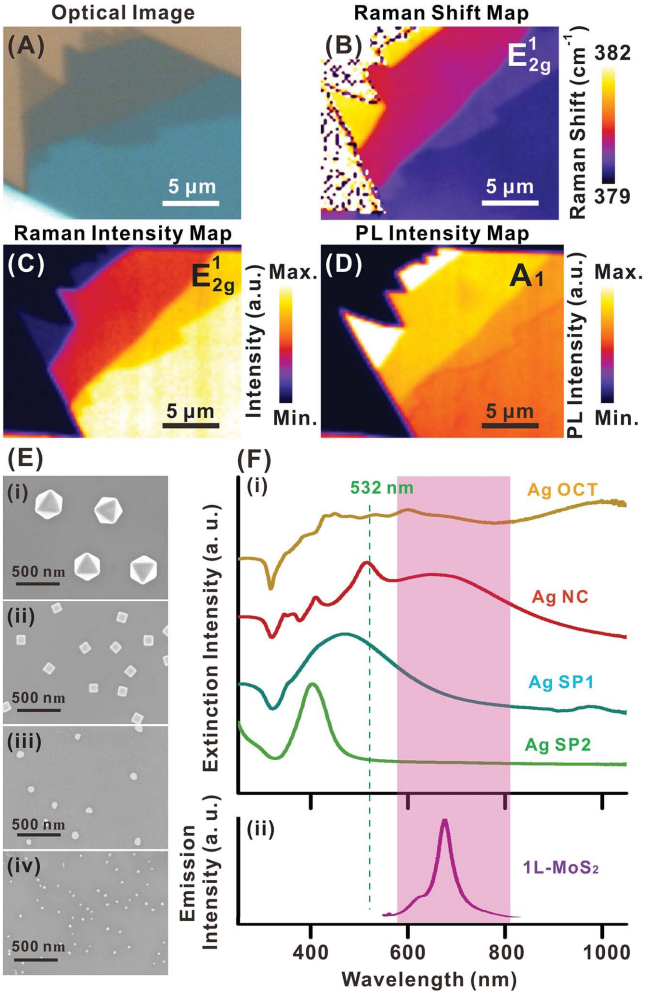

Figure 1. Characterization of MoS_2 flakes and Ag nanoantennas. A) Bright field optical microscope image of mechanically exfoliated (1L, 2L, 3L, 4L, and bulk) MoS_2 flakes on SiO_2/Si substrate. B) Raman shift map of MoS_2 flakes created using the E^1_{2g} peak frequency. C) Raman intensity map of MoS_2 flakes created using the E^1_{2g} (379.3 cm^{-1}) peak intensity. D) Photoluminescence intensity map of MoS_2 flakes created using the A_1 band (680 nm) intensity. E) SEM images of synthesized (i) Ag octahedra (Ag OCT), size: 340 ± 6 nm. ii) Ag nanocubes (Ag NC), size: 115 ± 5 nm. iii) Large Ag nanospheres (Ag SP1), size: 95 ± 10 nm. iv) Smaller Ag nanospheres (Ag SP2), size: 40 ± 4 nm. F) i) These extinction spectra overlap to varying extents with the (ii) emission spectra of 1L-MoS_2; dashed vertical line corresponds to the laser excitation wavelength.

Raman peak (E^1_{2g}, A_{1g}) frequency and intensity, as well as photoluminescence band (B_1, A_1) intensity, consistent with those reported in the literature (Figure 1B–D and Figure S1C–F, Supporting Information).[22,38]

In our system, we utilize the spectral overlap between the LSPRs of Ag nanoantennas and the bandgap of 1L-MoS_2 to couple the 1L-MoS_2 photoluminescence with the plasmon modes, followed by radiating to the far field through the plasmon resonance. This experimental design also enables us to tune the excitation enhancement efficiency, quantum yield, and emission directionality. To tailor this spectral overlap, we synthesize a library of Ag nanoparticles, including shape-controlled cubes (Ag NC), octahedra (Ag OCT), and spherical particles (Ag SP) of various sizes (Figure 1E). Ag OCT and NC are synthesized using the polyol reduction method,[39] whereas Ag SP of two different sizes are synthesized via the citrate-reduction method (Figure S2, Supporting Information).[40] The average edge lengths of Ag OCT and Ag NC are 340 ± 6 nm and 115 ± 5 nm, respectively (Figure S2A,B, Supporting Information). The diameters of Ag SP1 are 95 ± 10 nm (Figure S2C, Supporting Information), and that of Ag SP2 are 40 ± 4 nm (Figure S2D, Supporting Information).

Ag NC supports multiple strong and distinct LSPR bands across the visible spectrum, with the dipolar resonance directly overlapping with the bandgap of 1L-MoS_2.[41,42] Ag OCT exhibits more complex optical signature with higher-order resonances in the 400–650 nm range, while the mode observed at ≈1000 nm is mainly quadrupolar in nature.[39] Ag SP1 has a broad LSPR band centered at 460 nm, dominated by dipolar resonance, and Ag SP2 supports a dipole resonance centered at around 400 nm.[40] The LSPRs of these Ag nanoparticles overlap with the bandgap of 1L-MoS_2 to various extents (Figure 1F). The radiation pattern of the dipolar mode has a doughnut shape, where most energy is radiated along the direction perpendicular to the dipole axis. In contrast, the higher-order modes have radiation maxima and radiation energy distributed in several directions.[43] As such, the directionality of the dipolar mode is better than the higher-order modes.

To create hybrid plasmonic-semiconductor nanostructures, the Ag nanoantennas are separately drop-cast onto 1L-MoS_2. MoS_2 thickness is first verified using AFM imaging as well as Raman characterization (Figures S3 and S5C, Supporting Information). Individual plasmonic nanoantennas are sparsely distributed on the 1L-MoS_2 flakes, with the average interparticle distance larger than 1 μm to avoid plasmon coupling between adjacent nanoparticles (**Figure 2**A). This interparticle distance also ensures that only single plasmonic nanoparticles are excited within the laser excitation volume. We use 532 nm as the incident excitation wavelength, allowing us to control the efficiency of exciting the LSPRs of the Ag nanoantenna. At the same time, this excitation wavelength is well above both A_1 and B_1 excitons of MoS_2. The laser excitation intensity for all experiments is kept below 1×10^5 mW cm^{-2} to avoid photodamage of the ultrathin MoS_2 layers.

Photoluminescence intensity maps of the hybrid nanostructures demonstrate localized optical control over the 1L-MoS_2 photoluminescence in the presence of the plasmonic nanoparticles (Figure 2B and Figure S4, Supporting Information). For Ag NC-1L-MoS_2, both the photoluminescence maps of the B_1 (625 nm) and A_1 (680 nm) bands display strong photoluminescence enhancement at regions deposited with single Ag NC (Figure 2B(i),C(i)). Away from the NC-decorated areas, the photoluminescence intensity immediately returns to that of bare 1L-MoS_2 (Figure 2D(i) and Figure S4A, Supporting Information). The same phenomena can also be observed in the photoluminescence intensity maps of Ag SP1-1L-MoS_2 (Figure 2B(ii),C(ii),D(ii) and Figure S4B, Supporting Information), but almost no enhancement is observed for Ag SP2-1L-MoS_2 (Figure 2B(iii),C(iii),D(iii) and Figure S4C, Supporting Information). On the other hand, quenched photoluminescence is observed from Ag OCT-1L-MoS_2 (Figure 2B(iv),C(iv),D(iv) and Figure S4D, Supporting Information).

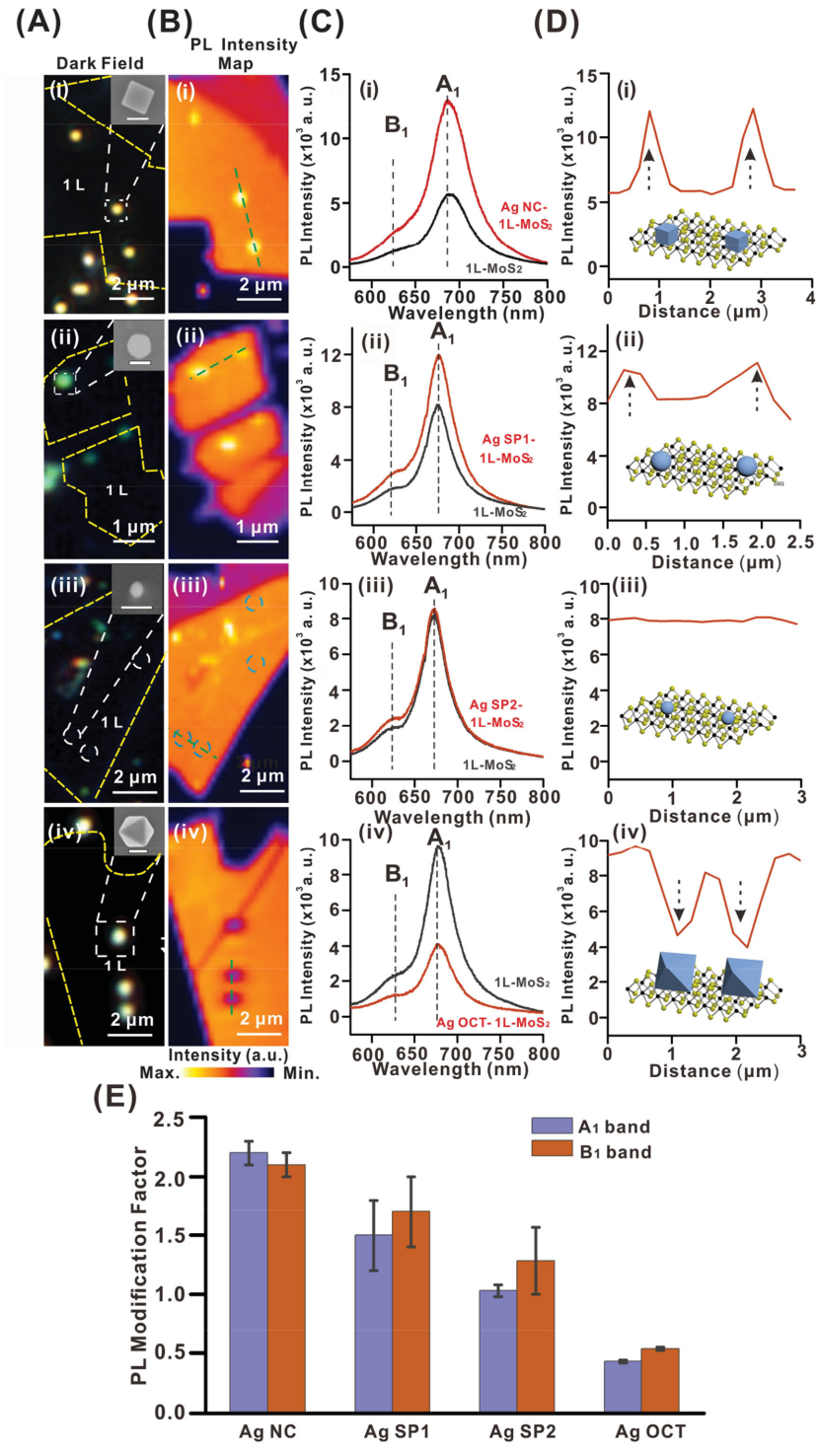

Figure 2. Tuning the photoluminescence of 1L-MoS_2 using various single shape-controlled Ag nanoantennas. A) Dark-field optical microscope image of exfoliated 1L-MoS_2 deposited with single (i) Ag NC, (ii) Ag SP1, (iii) Ag SP2, (iv) Ag OCT. Insets are SEM images of the respective single nanoantenna, scale bars are 100 nm in (i), (ii), (iii), and 200 nm in (iv). B) Photoluminescence intensity maps of 1L-MoS_2 deposited with single Ag nanoantenna created using A_1 peak (680 nm) intensity. C) Photoluminescence spectra of bare 1L-MoS_2 with and without the Ag nanoantenna. D) A_1 band intensity profile across green dashed line in (B). E) Modification factors for the photoluminescence bands (A_1, B_1) using different Ag nanoantennas.

We evaluate the photoluminescence modification factor (MF) using the following equation: Photoluminescence MF = Photoluminescence band intensity of Ag-MoS_2/ Photoluminescence band intensity of bare MoS_2. The presence of Ag NC enhances the photoluminescence of 1L-MoS_2 by an average of two-fold for both emission bands (≈2.1 ± 0.1 and 2.2 ± 0.1 for B_1 and A_1 bands, respectively; Figure 2E). Similar enhancement is observed for Ag SP1, with the MF calculated to be ≈1.6-fold (≈1.7 ± 0.3 and 1.5 ± 0.3 for B_1 and A_1 bands, respectively). The MF approaches 1 for Ag SP2-1L-MoS_2 and reduces to less than 0.5-fold for Ag OCT-1L-MoS_2.

The plasmonic mediation of Ag nanoantennas on the emission of 1L-MoS_2 is the combined result of excitation enhancement, emission modification, and altered emission directionality, which can be described by the following equation[44]

$$\mathrm{MF} = \frac{\eta}{\eta_0}\frac{\gamma_{ex}}{\gamma_{ex}^0}\frac{\mathrm{QY}}{\mathrm{QY}_0} \quad (1)$$

where the η, γ_{ex}, and QY are the photoluminescence collection efficiencies, excitation rate, and quantum yield of the sample with Ag nanoantennas, respectively; η_0, γ_{ex}^0, and QY_0 are the photoluminescence collection efficiencies, the excitation rates, and quantum yield of sample without Ag nanoantennas. $\frac{\gamma_{ex}}{\gamma_{ex}^0}$ is proportional to the electric field intensity enhancement, $|E_{inc}^2|/|E_0^2|$, at the excitation wavelength.

In the Ag NC-1L-MoS_2 case, the LSPRs overlap completely with both the laser excitation wavelength (532 nm) and the bandgap of 1L-MoS_2 (680 nm), resulting in significant field enhancement at both the laser excitation and 1L-MoS_2 emission wavelengths. From electrodynamic simulations performed using the finite-difference time-domain approach, the largest field enhancements ($|E_{inc}^2|/|E_0^2|$) for Ag NC are 950-fold and 720-fold at 532 and 680 nm, respectively (**Figures 3**A(i) and **4**B(i)). The excitation rate is therefore enhanced up to 950-fold at the largest field sites. Electrodynamic calculations show that the photoluminescence quantum yield of 1L-MoS_2 can be enhanced by 13.9-fold at the largest field sites of Ag NC. In addition, the photon collection efficiency is only slightly decreased from 15% to 13% in the presence of Ag NC (Figure 3C). As such, a maximum of up to 10^4 enhancement in photoluminescence is derived from the Ag

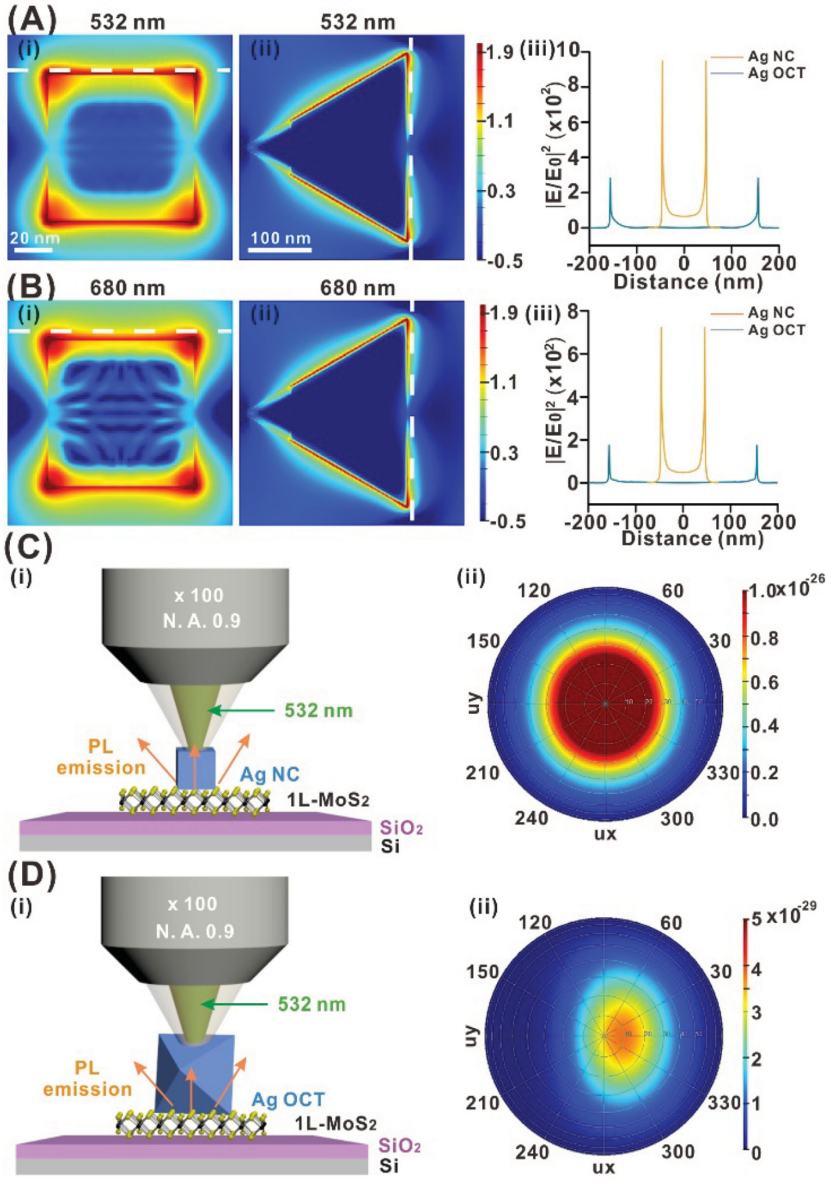

Figure 3. Simulation of local electromagnetic field distribution and far-field emission pattern of single Ag nanocube/octahedra on 1L-MoS_2. Local electromagnetic field enhancement distributions derived from (i) Ag NC, (ii) Ag OCT on 1L-MoS_2, and (iii) extracted field distribution profile across the dashed line at the A) excitation wavelength of 532 nm and B) the emission peak of 680 nm. C) i) Scheme of detecting photoluminescence of Ag NC-1L-MoS_2 and (ii) simulation of Ag NC-coupled far-field emission pattern. D) i) Scheme of detecting photoluminescence of Ag OCT-1L-MoS_2 and (ii) simulation of Ag OCT-coupled far-field emission pattern.

NC-1L-MoS_2 system near the cube vertices. However, these largest field enhancements are confined to the vertices of Ag NC. Consequently, a relatively small enhancement is obtained in our experiments. The large field enhancement at the laser excitation wavelength enables Ag NC to serve as localized nanoscale optical pumps to increase photon absorption and the generation rate of electron–hole pairs in 1L-MoS_2. Furthermore, significant field enhancement at the 1L-MoS_2 emission wavelength can accelerate the radiative decay through the Purcell effect. The coupled emission between the radiative dipole resonance of Ag NC and 1L-MoS_2 is optimal, leading to enhanced emission.

As the nanoparticles change from NC to SP1 and SP2, the overlaps between the plasmon resonances and the laser excitation as well as that between the plasmon resonances and 1L-MoS_2 bandgap decrease, leading to lower efficiency of exciting the LSPRs. Such off-resonant excitation leads to progressively smaller photoluminescence MF calculated for the various samples. An indirect evidence of this phenomenon is evident from the enhanced Raman scattering signals of 1L-MoS_2 in the presence of Ag nanoantenna (Figure S5, Supporting Information), which show a nanoparticle-dependent trend of Raman intensity enhancement following that of the photoluminescence enhancement.

In contrast, photoluminescence weakening of 1L-MoS_2 using Ag OCT arises from both the emission quenching and the more complex antenna effect of Ag OCT. Weaker maximum field enhancements of 280-fold and 170-fold are observed at the laser excitation 1L-MoS_2 emission wavelengths for Ag OCT-1L-MoS_2, respectively (Figures 3A(ii) and 4B(ii)). The field enhancement at the excitation wavelength gives rise to an excitation rate enhancement of 280-fold. Although the electric field at the emission wavelength is enhanced by 170-fold, the quantum yield is reduced to 0.2-fold of the original emission in the presence of Ag OCT. This reduction arises from the non-radiative nature of the high-order plasmon resonances. In addition, because of the poor directionality of high-order plasmon modes, we find that the collection efficiency is reduced from 15% to 0.26% by Ag OCT (Figure 3D). Taking all effects together, Ag OCT gives rise to an enhancement factor of 0.89 at the largest electric field enhancement positions. Since the strongest fields are localized at the particle vertices, even lower enhancement is expected over the particle surfaces. Therefore, the overall effect of Ag OCT on the photoluminescence of 1L-MoS_2 is emission weakening.

Notably, the intrinsic spectral properties of 1L-MoS_2 remain practically unchanged in the presence of Ag nanoantenna with only a slight red-shift even under increased excitation power (Figure S6A,B, Supporting Information). In addition, the photoluminescence enhancement is independent of excitation power (Figure S6C,D, Supporting Information), suggesting that photothermal heating is insignificant in our system compared to a previous study.[31]

In addition, Ag NC is also able to enhance the emission of multilayered indirect bandgap MoS_2 flakes (both 2L and 3L; Figure S7, Supporting Information). The photolumines-

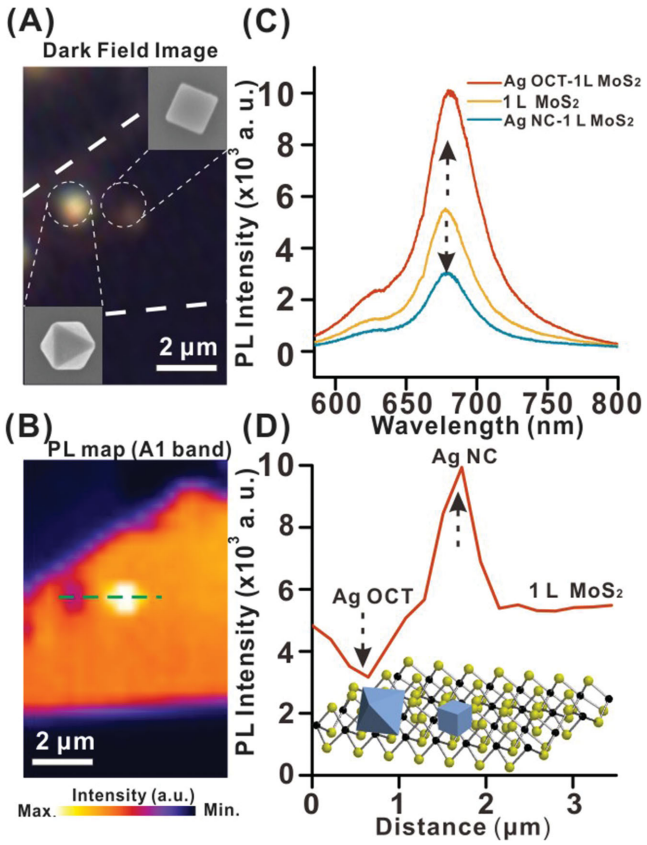

Figure 4. Realizing a heterogeneous optical platform with tunable photoluminescence signals on a single 1L-MoS_2 flake. A) Dark-field image of 1L-MoS_2 deposited with both single Ag NC and OCT. B) Corresponding photoluminescence intensity map at A_1 band position shows dramatically tailored photoluminescence signals. C) Photoluminescence spectra of Ag OCT-1L-MoS_2, Ag NC-1L-MoS_2, and 1L-MoS_2 extracted from the photoluminescence map. D) A_1 band photoluminescence intensity profile across green dashed line labeled position in (B).

cence MF for 2L-MoS_2 is estimated to be ≈1.5 (1.4 ± 0.1 and 1.5 ± 0.1 for B_1 and A_1 bands, respectively, Figures S7F and S8, Supporting Information). For 3L-MoS_2, the average photoluminescence MF is ≈1.3 (1.2 ± 0.1 and 1.3 ± 0.1 for B_1 and A_1 bands, respectively, Figures S7G and S8, Supporting Information). The decreased MF value (Figure S8, Supporting Information) is due to a decrease in emission efficiency with increasing layer thickness.

To realize an optical platform with tunable and heterogeneous photoluminescence output, we deposit both Ag NC and OCT on a single 1L-MoS_2 flake (Figure 4A). The co-existence of both types of nanoantennas gives rise to 1L-MoS_2 flake with multiple photoluminescence intensities (Figure 4B–D). The extent of emission enhancement and quenching is similar to the individual systems (Figure 4C). Earlier studies have focused mainly on using bulk lithographically fabricated structures to control the "ensemble" optical emission of 1L-MoS_2, hence precluding the ability to modify the photoluminescence of 1L-MoS_2 at the nanoscale. Furthermore, these studies have only been able to separately achieve either photoluminescence enhancement or quenching but not both within the same system. In our experiment, we not only tune the optical response of 1L-MoS_2 through the use of different Ag nanoantennas, but further enable the realization of an optical platform with multiple highly confined signal emission. This opens up new approaches to design nanoscale optoelectronic devices and at the same time, suggests the use of this platform in fields such as data storage[21] and circuit integration.[19]

Our work successfully demonstrates the creation of a heterogeneous optical platform built upon the integration of plasmonic nanoantenna with 1L-MoS_2, achieved via a localized control over the photoluminescence emission of 1L-MoS_2 using single Ag nanoantenna. The emission intensity is highly tunable, and can be easily manipulated via a judicious selection of nanoantenna morphology. As the nanoantenna changes from nanocubes to octahedra, the photoluminescence intensity changes from an enhanced to a weakened state. This phenomenon arises from LSPR-based excitation enhancement and from the morphology-dependent antenna effect of the various plasmonic nanoantennas. By simultaneously introducing both Ag NC and Ag OCT, we are able to create a heterogeneous optical platform with a tunable range of photoluminescence signals, concurrently observing the base photoluminescence from 1L-MoS_2, as well as enhanced and weakened emissions in the presence of the respective Ag nanoantenna. Such unprecedented nanoscale control coupled with highly tailorable optical output is promising for the integration of transition metal dichalcogenide-based optoelectronics. Furthermore, our Ag nanoantenna can be used to enhance photoluminescence on few-layer indirect bandgap MoS_2.

Supporting Information

Supporting Information is available from the Wiley Online Library or from the author.

Acknowledgements

X.Y.L. and Y.H.L. thank the National Research Foundation, Singapore (NRF-NRFF2012-04), and the Nanyang Technological University's start-up grant (M4080758) for support. J.F.W. acknowledges support from Hong Kong RGC CRF (Ref. No. CUHK4/CRF/12G). T.X.L. and W.G. are grateful for support from the National Natural Science Foundation of China (51125011, 51433001). W.G. thanks the China Scholarship Council (CSC) for support.

Received: August 11, 2015
Revised: October 15, 2015
Published online: November 26, 2015

[1] A. G. Curto, G. Volpe, T. H. Taminiau, M. P. Kreuzer, R. Quidant, N. F. van Hulst, *Science* **2010**, *329*, 930.
[2] M. A. Schreuder, K. Xiao, I. N. Ivanov, S. M. Weiss, S. J. Rosenthal, *Nano Lett.* **2010**, *10*, 573.
[3] K. Okamoto, I. Niki, A. Shvartser, Y. Narukawa, T. Mukai, A. Scherer, *Nat. Mater.* **2004**, *3*, 601.
[4] W. Zhou, J. Lee, J. Nanda, S. T. Pantelides, S. J. Pennycook, J.-C. Idrobo, *Nat. Nanotechol.* **2012**, *7*, 161.

[5] A. Schiffrin, T. Paasch-Colberg, N. Karpowicz, V. Apalkov, D. Gerster, S. Muhlbrandt, M. Korbman, J. Reichert, M. Schultze, S. Holzner, J. V. Barth, R. Kienberger, R. Ernstorfer, V. S. Yakovlev, M. I. Stockman, F. Krausz, *Nature* **2013**, *493*, 70.
[6] G. Eda, S. A. Maier, *ACS Nano* **2013**, *7*, 5660.
[7] Y. Cui, I. Y. Phang, Y. H. Lee, M. R. Lee, Q. Zhang, X. Y. Ling, *Chem. Commun.* **2015**, *51*, 5363.
[8] Y. Cui, R. S. Hegde, I. Y. Phang, H. K. Lee, X. Y. Ling, *Nanoscale* **2014**, *6*, 282.
[9] J. A. Schuller, E. S. Barnard, W. Cai, Y. C. Jun, J. S. White, M. L. Brongersma, *Nat. Mater.* **2010**, *9*, 193.
[10] T. Kosako, Y. Kadoya, H. F. Hofmann, *Nat. Photonics* **2010**, *4*, 312.
[11] N. P. de Leon, B. J. Shields, L. Y. Chun, D. E. Englund, A. V. Akimov, M. D. Lukin, H. Park, *Phys. Rev. Lett.* **2012**, *108*, 226803.
[12] H. A. Atwater, A. Polman, *Nat. Mater.* **2010**, *9*, 205.
[13] T. Ming, H. Chen, R. Jiang, Q. Li, J. Wang, *J. Phys. Chem. Lett.* **2012**, *3*, 191.
[14] T. Ming, L. Zhao, H. Chen, K. C. Woo, J. Wang, H.-Q. Lin, *Nano Lett.* **2011**, *11*, 2296.
[15] A. Kinkhabwala, Z. Yu, S. Fan, Y. Avlasevich, K. Müllen, W. Moerner, *Nat. Photonics* **2009**, *3*, 654.
[16] W. Zhou, M. Dridi, J. Y. Suh, C. H. Kim, D. T. Co, M. R. Wasielewski, G. C. Schatz, T. W. Odom, *Nat. Nanotechnol.* **2013**, *8*, 506.
[17] R.-M. Ma, R. F. Oulton, V. J. Sorger, G. Bartal, X. Zhang, *Nat. Mater.* **2011**, *10*, 110.
[18] R. F. Oulton, V. J. Sorger, T. Zentgraf, R.-M. Ma, C. Gladden, L. Dai, G. Bartal, X. Zhang, *Nature* **2009**, *461*, 629.
[19] N. Engheta, *Science* **2007**, *317*, 1698.
[20] B. Radisavljevic, A. Kis, *Nat. Mater.* **2013**, *12*, 815.
[21] Y. Cui, I. Y. Phang, R. S. Hegde, Y. H. Lee, X. Y. Ling, *ACS Photon.* **2014**, *1*, 631.
[22] A. Splendiani, L. Sun, Y. Zhang, T. Li, J. Kim, C.-Y. Chim, G. Galli, F. Wang, *Nano Lett.* **2010**, *10*, 1271.
[23] O. Lopez-Sanchez, D. Lembke, M. Kayci, A. Radenovic, A. Kis, *Nat. Nanotechol.* **2013**, *8*, 497.
[24] S. Ghatak, A. N. Pal, A. Ghosh, *ACS Nano* **2011**, *5*, 7707.
[25] B. Radisavljevic, A. Radenovic, J. Brivio, V. Giacometti, A. Kis, *Nat. Nanotechnol.* **2011**, *6*, 147.
[26] O. Salehzadeh, N. H. Tran, X. Liu, I. Shih, Z. Mi, *Nano Lett.* **2014**, *14*, 4125.
[27] Z. Li, R. Ye, R. Feng, Y. Kang, X. Zhu, J. M. Tour, Z. Fang, *Adv. Mater.* **2015**, *27*, 5235.
[28] S. Mouri, Y. Miyauchi, K. Matsuda, *Nano Lett.* **2013**, *13*, 5944.
[29] P. Joo, K. Jo, G. Ahn, D. Voiry, H. Y. Jeong, S. Ryu, M. Chhowalla, B.-S. Kim, *Nano Lett.* **2014**, *14*, 6456.
[30] H. Nan, Z. Wang, W. Wang, Z. Liang, Y. Lu, Q. Chen, D. He, P. Tan, F. Miao, X. Wang, *ACS Nano* **2014**, *8*, 5738.
[31] S. Najmaei, A. Mlayah, A. Arbouet, C. Girard, J. Léotin, J. Lou, *ACS Nano* **2014**, *8*, 12683.
[32] S. Butun, S. Tongay, K. Aydin, *Nano Lett.* **2015**, *15*, 2700.
[33] A. Sobhani, A. Lauchner, S. Najmaei, C. Ayala-Orozco, F. Wen, J. Lou, N. J. Halas, *Appl. Phys. Lett.* **2014**, *104*, 031112.
[34] Z. Li, Y. Xiao, Y. Gong, Z. Wang, Y. Kang, S. Zu, P. M. Ajayan, P. Nordlander, Z. Fang, *ACS Nano* **2015**, *9*, 10158.
[35] Y. Kang, Y. Gong, Z. Hu, Z. Li, Z. Qiu, X. Zhu, P. M. Ajayan, Z. Fang, *Nanoscale* **2015**, *7*, 4482.
[36] Y. Kang, S. Najmaei, Z. Liu, Y. Bao, Y. Wang, X. Zhu, N. J. Halas, P. Nordlander, P. M. Ajayan, J. Lou, *Adv. Mater.* **2014**, *26*, 6467.
[37] U. Bhanu, M. R. Islam, L. Tetard, S. I. Khondaker, *Sci. Rep.* **2014**, *4*, 5575.
[38] C. Lee, H. Yan, L. E. Brus, T. F. Heinz, J. Hone, S. Ryu, *ACS Nano* **2010**, *4*, 2695.
[39] a) A. Tao, P. Sinsermsuksakul, P. Yang, *Angew. Chem.* **2006**, *118*, 4713; *Angew. Chem. Int. Ed.* **2006**, *45*, 4597.
[40] N. G. Bastús, F. Merkoçi, J. Piella, V. Puntes, *Chem. Mater.* **2014**, *26*, 2836.
[41] C. Fang, Y. H. Lee, L. Shao, R. Jiang, J. Wang, Q.-H. Xu, *ACS Nano* **2013**, *7*, 9354.
[42] Y. H. Lee, H. Chen, Q.-H. Xu, J. Wang, *J. Phys. Chem. C* **2011**, *115*, 7997.
[43] P. Biagioni, J.-S. Huang, B. Hecht, *Rep. Prog. Phys.* **2012**, *75*, 024402.
[44] G. M. Akselrod, T. Ming, C. Argyropoulos, T. B. Hoang, Y. Lin, X. Ling, D. R. Smith, J. Kong, M. H. Mikkelsen, *Nano Lett.* **2015**, *15*, 3578.